SI Appendix for:

Title (max 135 characters including spaces, comprehensible to broad audience):

Stable Solar-Driven Oxidation of Water by Semiconducting Photoanodes Protected by Transparent Catalytic Nickel Oxide Films

Short Title (for mobile devices and RSS feeds, < 50 characters including spaces):

Stable Water Oxidation by NiO_x-Coated Photoanodes

Authors:

Ke Sun[a,b], Fadl H. Saadi[b,c], Michael F. Lichterman[a,b], William G. Hale[b,d], Hsin-ping Wang[e], Xinghao Zhou[b,c], Noah T. Plymale[a], Stefan T. Omelchenko[b,c], Jr-Hau He[e], Kimberley M. Papadantonakis[a,b], Bruce S. Brunschwig[b,f], Nathan S. Lewis [a,b,f,g,1]

Author Affiliations:

[a]Division of Chemistry and Chemical Engineering, California Institute of Technology, Pasadena, CA 91125, USA

[b]Joint Center for Artificial Photosynthesis, California Institute of Technology, Pasadena, CA 91125, USA

[c]Division of Engineering and Applied Sciences, California Institute of Technology, Pasadena, CA 91125, USA

[d]Department of Chemistry, University of Southampton, Southampton, Hampshire, SO17 1BJ UK

[e]Computer, Electrical and Mathematical Sciences and Engineering (CEMSE) Division, King Abdullah University of Science & Technology (KAUST), Thuwal 23955-6900, Saudi Arabia

[f]Beckman Institute Molecular Materials Research Center, California Institute of Technology, Pasadena, CA 91125, USA

[g]Kavli Nanoscience Institute, California Institute of Technology, Pasadena, CA 91125, USA

SI Appendix

Text S1**:**

Preparation of Samples:

Chemicals:

Except where otherwise noted, all materials were used as received, including sulfuric acid (H_2SO_4, J. T. Baker, ACS reagent, 95%-98%), concentrated hydrochloric acid (HCl, Sigma Aldrich, ACS Reagent 37%), hydrogen peroxide (H_2O_2, Macron Chemicals, ACS grade 30%), concentrated ammonium hydroxide (NH_4OH, Sigma Aldrich, ACS reagent 28%-30%), buffered HF improved (Transene Company Inc.), potassium hydroxide pellets (KOH, Macron Chemicals, ACS 88%), potassium ferrocyanide trihydrate ($K_4Fe(CN)_6 \cdot 3H_2O$, Acros, >99%), potassium ferricyanide ($K_3Fe(CN)_6$, Fisher Chemicals, certified ACS 99.4%), potassium chloride (KCl, Macron Chemicals, Granular ACS 99.6%), monobasic potassium phosphate (HK_2PO_4, Fisher Scientific, ACS >99%), dibasic potassium phosphate (H_2KPO_4, Fisher Scientific, ACS >99%), cobalt(II) nitrate ($Co(NO_3)_2$, Acros, ACS >99%), Br_2 (Sigma Aldrich, 99.999%), and CH_3OH (EMD Millipore, >99.9%). Water with a resistivity of 18.2 MΩ·cm was obtained from a Millipore deionized water system.

Preparation of substrates:

Boron degenerately doped (p^+-type, resistivity <0.005 Ω·cm, single-side polished, (111)-oriented) Si wafers were purchased from Addison Engineering. The Si wafers were cleaned in buffered oxide etchant, typically for 30-45 s, until the surface was hydrophobic. The samples

were then immersed for 30 min in mixture of 1:1:5 (v/v) of H_2O_2:HCl:H_2O at 70 °C, and were subsequently thoroughly rinsed using deionized H_2O and dried using N_2(g). Before loading into the sputtering chamber, samples were etched with buffered HF(aq) to remove native oxides, rinsed with deionized H_2O, and dried using N_2(g).

As-cut Czochralski n-type monocrystalline Si (100-oriented, double-side polished, with a dopant density of 10^{17} cm^{-3}) wafers with thickness of 200 μm were used for fabrication of the HTJ-Si cells. First, Si micropyramids were fabricated via an anisotropic etching process at 85 °C for 20 min using an aqueous solution of KOH and isopropyl alcohol in water with a volume ratio of 1:1:17. Then, plasma-enhanced chemical-vapor deposition (PECVD) of an intrinsic *a*-Si:H buffer layer (5 nm) with a p-type *a*-Si:H layer (6 nm) on top as emitter layers was performed at 150 ˚C, and an intrinsic *a*-Si:H buffer layer (5 nm) with an n-type *a*-Si:H layer (10 nm) was deposited on the back, to serve as surface-field layers, under a typical growth rate of 1.5 Å s^{-1}. Samples were stored in N_2(g) before etching in buffered HF(aq) to remove the surface native oxide, rinsed with deionized water, and dried using N_2(g). Samples were then loaded into the sputtering chamber immediately for deposition of NiO_x.

CdTe pieces were cut from n-CdTe (111-oriented, double-side polished, with a dopant density of 5.5×10^{17} cm^{-3}) wafers. Pieces of the CdTe were etched for 30 s in a freshly prepared solution of Br_2 dissolved in CH_3OH (0.04% v/v). The samples were then rinsed vigorously with CH_3OH, and immersed in CH_3OH until being dried using N_2(g) before being placed in the sputtering chamber for deposition of NiO_x.

The *a*-Si:H films were prepared by RF decomposition of silane, and were all prepared at HT Products by H. Wiesmann. The In-doped SnO_2 (ITO) substrate was maintained at 220℃ with a deposition rate of 1.5 Å s^{-1}. A 200 Å thick n-doped layer was deposited from silane with 1% phosphine, and was then followed by a nominally intrinsic 0.5-0.6 μm layer of *a*-Si:H(1, 2). *a*-Si:H samples were cleaned in buffered HF(aq) until the surface was hydrophobic, typically

requiring ~30-45 s. The samples were then immersed in a mixture of 1:1:5 (v/v) H_2O_2:HCl:H_2O for 30 min at 70 °C. The samples were then thoroughly rinsed with H_2O and dried using N_2(g) before being transferred into the sputtering chamber for NiO_x deposition.

GaAs pieces were cut from n^+-GaAs (100-oriented, carrier concentration 10^{18} cm^{-3}, single-side polished) wafers obtained from AXT, Inc. The pieces were etched for 30 s in a freshly prepared solution of 0.04% (v/v) Br_2/CH_3OH solution and were thoroughly rinsed with CH_3OH, then etched in 1.0 M NaOH(aq) for 15 s, rinsed with deionized water, and dried using N_2(g) before being placed in a sputtering chamber for deposition of NiO_x.

NiO_x sputtering deposition:

Reactive RF sputtering using an AJA high-vacuum magnetron sputtering system (AJA International Inc.) was conducted in a chamber with a maximum base pressure of 8×10^{-8} Torr. The O_2 concentration was varied from 0 to 0.33 with a constant Ar flow of 20 standard cubic centimeter per minute (sccm) while the working pressure was held at 5 mTorr. The substrates were maintained at 300 °C. The deposition rate was maintained at 0.2 Å s^{-1} by tuning the sputtering power on the Ni target (Kurt Lesker, 2" diameter × 0.125" thickness, 99.95%). To deposit metallic Ni, a constant RF power of 150 W was used without substrates heating or O_2 gas supply.

Text S2:

Characterization of Samples

X-ray photoelectron spectroscopy (XPS)

XPS data were obtained using an AXIS Ultra DLD instrument (Kratos Analytical, Manchester, UK) at a background pressure of 1×10^{-9} Torr. High-intensity excitation was provided by monochromatic Al Kα X-rays, 1486.6 eV in energy and 0.2-eV resolution at full width at half maximum. For the Fe 2p high resolution scans, Mg Ka X-rays of 1253.7 eV were used instead in order to minimize the overlapping of Ni Auger peaks with the Fe 2p peaks. Photoelectrons were collected at 0º from the surface normal at a retarding (pass) energy of 80 eV for the survey scans, whereas a pass energy of 20 eV was used for the high-resolution scans. The peak energies were calibrated against the binding energy, E_B, of the adventitious C 1s peak (taken to be 284.8 eV).

X-ray diffraction spectroscopy

XRD analysis was conducted using a Bruker D8 Discover system equipped with a 2-dimensional Vantec-500 detector. Cu-Kα radiation (1.54 Å) was generated at a tube voltage of 1 kV and a tube current of 50 mA. The incident beam was focused using a mono-capillary collimator. A laser beam marked the focal spot on the specimen that was fixed on an xyz stage. The scattered diffraction was registered by a 2-dimensional detector with the angular resolution of the detector smaller than 0.04°, and enabled the simultaneous detection of the diffraction data in a 2θ range of 20°. The detected radiation was counted for 2000 s to obtain an appropriate XRD profile. The data were analyzed using Bruker EVA software.

UV-vis reflectance and transmittance measurement:

The optical reflectance and transmittance of the NiO_x- or Ni metal-coated Si and HTJ-Si substrates were determined by using an integrating sphere at normal incidence (Agilent Cary 5000 UV-Vis spectrometer). The absorptance (A) of NiO_x-coated Si was calculated from the

measured total reflectance (R) and transmittance (T) of the electrode as $A = 1 - R - T$. All optical measurements were done in air on fresh samples without chemical/electrochemical treatment.

Preparation of electrodes:

Ohmic contacts were formed by scribing an In-Ga eutectic alloy (Alfa Aesar, 99.99%) to the back side of the HTJ-Si cell and to the p^+-Si substrates. To form an ohmic contact to n-CdTe and n^+-GaAs, In was soldered onto the back side of the sample. Ohmic contact for *a*-Si was made by scribing In-Ga across the *a*-Si:H to the bottom In-doped Sn oxide (ITO) substrate. High-purity Ag paint (SPI supplies) was then used to mechanically attach the ohmic contact to a coiled, tin-plated Cu wire (McMaster-Carr) which was then threaded through a glass tube (Corning Incorporated, Pyrex tubing, 7740 glass). The sample was encapsulated and sealed to the glass tube using a mixture of 2:1 grey epoxy (Hysol 9460F) and white epoxy (Hysol 1C). The epoxy was allowed to dry under ambient conditions for at least 12 h. A high-resolution optical scanner (Epson Perfection V370 with a resolution of 2400 psi) was used to image the exposed surface area of each electrode, and the geometric areas were determined by analyzing the images using ImageJ software. All of the electrodes in this study were 0.1-0.2 cm^2 in area, unless specified otherwise.

Preparation of HTJ-Si|ITO|Co-Pi photoanode and FTO|Co-Pi dark electrode:

Indium doped tin oxide (ITO) with a thickness of 90 nm was deposited on the front and back of the HTJ-Si using sputtering. Front and back contacts were made by using Ag paste to attach a Cu wire to the front and back ITO layers, respectively. Wire contacts and epoxy were made on the edges on the front contacts, while the entire back contacts were isolated by epoxy. The Co-phosphate precursor solution was 0.1 M potassium phosphate (K-Pi, a mixture of 61.5%

0.1 M dibasic K_2HPO_4 and 38.5% 0.1 M monobasic KH_2PO_4) and 0.5 mM cobalt nitrate. Electrodeposition was performed in a two-compartment cell with the front ITO on the HTJ-Si as the working electrode and a fritted Pt mesh as a counter electrode, with a saturated calomel electrode (SCE, 0.654 V vs. RHE) as the reference electrode. Deposition of the Co catalyst precursor in various thicknesses was performed with agitation under a constant current density of 1 mA cm^{-2} by passing various amounts of charge (30 to 1800 mC cm^{-2}). Samples were then rinsed with DI-H_2O and dried under a stream of N_2(g). The transmittance of Co-Pi coated FTO substrates was measured prior to the electrochemical measurement. The samples were then transferred to 0.1 M K-Pi(aq) and then to 1.0 M KOH(aq) for electrochemical measurements. The photoelectrochemical measurement of an HTJ-Si|ITO|CoO_x electrode was conducted through the back contact under simulated 1-Sun illumination in 1.0 M KOH(aq). Detailed electrochemical measurement setup can be found in the section below. The stability data for this system were obtained using the same protocol as for all of the NiO_x-protected photoanodes evaluated herein described in the section below.

Electrochemical measurements:

A Mercury/Mercury oxide (Hg/HgO in 1.0 M KOH(aq), CH Instruments, CH152) electrode was used as the reference electrode, and a carbon cloth placed within a fritted glass tube (gas dispersion tube Pro-D, Aceglass, Inc.) was used as the counter electrode for all electrochemical measurements performed in 1.0 M KOH(aq) electrolyte, including photoelectrochemical, spectral response, and faradaic efficiency measurements. The Hg/HgO reference electrode was calibrated versus the reversible hydrogen electrode and the Hg/HgO electrode potential was determined to be 0.926 V vs. RHE. The equilibrium potential for the oxygen-evolution reaction was therefore 0.304 V vs the Hg/HgO reference. A custom electrochemical cell with a flat glass (Pyrex) bottom was used for all of the electrochemical

measurements. During measurements, the electrolyte was vigorously agitated with a magnetic stir bar driven by a model-train motor (Pittman) with a Railpower 1370 speed controller (Model Rectifier Corporation). The data presented for photoelectrochemical measurements in aqueous solutions do not include compensation for the series resistance of the solution. To evaluate the catalytic activity, correction for the solution resistance was applied. ELH-type (Sylvania/Osram) and ENH-type (EIKO) tungsten-halogen lamps with a custom housing and with a transformer (Staco Energy Products Co.) were used for long-term photoelectrochemical stability measurements. A Xe arc lamp (Newport 67005 and 69911) equipped with an IR filter (Newport 61945) and with an AM 1.5 filter (Newport 81094 and 71260) was used as the light source for *J-E* measurements and for the spectral response measurements. The illumination intensity at the position of the working electrode in the electrochemical cell was determined by placing a calibrated Si photodiode (FDS100-Cal, Thor Labs) into the cell at the same position occupied by the exposed area of the photoelectrode. To illuminate bottom-facing photoelectrodes, a quartz diffuser (Newport 15Diff-Vis) together with a broadband reflection mirror (Newport dielectric mirror, 10Q20PR-HR) was used to direct the uniform light beam from the horizontal to the vertical direction.

Cyclic voltammetry as well as quantum yield data were obtained using a Biologic SP-200 potentiostat (Bio-Logic Science Instrument). The cyclic voltammetric data were recorded at a constant scan rate of 40 mV s^{-1} with a scan range that varied depending on the photovoltage of the sample. The external quantum yield was collected using the potentiostat connected to a lock-in amplifier with the light chopped at 20 Hz.

Photoanode water-oxidation stability-measurement protocols:

Stability measurements were performed in 1.0 M KOH(aq) under simulated 1-Sun illumination using an ENH-type tungsten halogen lamp with a dichroic rear reflector. The

electrochemical cell was continually cooled by flowing compressed air on the sidewall of the cell. The electrolyte in the cell, as well as in the Hg/HgO reference electrode, was changed every 24-48 h to prevent concentrating species within the cell solution and to prevent system over-loading caused by the presence of gas bubbles in the reference electrodes, as well as to maintain a stable reference potential. The reference electrode was calibrated during the course of the measurement using the method described above. The light intensity at the sample position was also calibrated whenever the electrolyte was replaced. A transformer was used to lower the voltage supply on the bulb to 40-50 V_{ac} to improve the lifetime of the bulb and to reduce the generation of heat. The light bulb was changed every 200-300 h to prevent unexpected bulb burn-out. The stability of the light source was also monitored by placing a Si reference photodiode at a fixed position relative to the lamp. An automatic data-collection protocol was implemented using the Biologic potentiostat such that 10 cyclic voltammetric scans were collected after every 10 h of chronoamperometric stability measurements. To minimize the change in conditions of the electrode when switching between chronomperometric and cyclic voltammetric measurements, the cyclic voltammteric measurement was set to use an initial and a final potential of 1.73 V vs. RHE, which was the potential used for chronoamperometry. The potential was then scanned between E_{low} and E_{high}. where E_{high} was fixed at 1.93 V vs. RHE and E_{low} was set depending on the photovoltage of the photoelectrodes, with E_{low} = 0.63 V vs. RHE for HTJ-Si|NiO_x and E_{low} = 0.83 V vs. RHE for CdTe|NiO_x and a-Si:H|NiO_x photoelectrodes.

Measurement of Faradaic efficiency:

A Neofox fluorescence probe (Foxy probe, Ocean Optics) was used to monitor the concentration of O_2 throughout the experiment. The fluorescence response was calibrated against the standard concentration of oxygen in water (7700 μg L^{-1} or 2.4×10^{-4} M) under a standard atmosphere that contained 20.9% (by volume) O_2(g). The fluorescence probe, the Hg/HgO/1.0 M

KOH reference electrode, a fritted Pt mesh counter electrode (Alfa-Aesar, 100 mesh, 99.9% trace metal basis), and the NiO_x-coated semiconductor working electrodes with a geometric surface area of 0.84-0.87 cm^2 (HTJ-Si|NiO_x), 0.12-0.22 cm^2 (*a*-Si:H|NiO_x), and 0.07 cm^2 (n-CdTe|NiO_x) were loaded into an airtight glass cell that had a volume of 43.6 mL with no headspace, and that was equipped with four ports and a side-facing quartz window. The cell and the 1.0 M KOH(aq) electrolyte in the cell were purged with a stream of ultra-high purity Ar(g) for ~1 h prior to the measurement of the O_2 produced by the electrode maintained in the water bath to minimize the temperature fluctuation during illumination. The current density was maintained at 1 mA cm^{-2} or lower, to prevent bubble formation on the electrode surfaces. The fluorescence probe was kept in the dark during the measurement. To compare the charge-versus-time data from the potentiostat with the amount of oxygen generated versus time for a system operating at 100% faradaic efficiency, the charge passed (in mA·h) was multiplied by 3.6 to convert the data into coulombs, and the result was then multiplied by 83 (the factor for conversion of 1 C of electrons to 1 μg of O_2) to convert the value into micrograms of O_2.

Spectroscopic ellipsometry and data fitting:

Thin films of Ni oxide backed by Si were investigated by use of a variable-angle spectroscopic ellipsometer with a rotating analyzer and equipped with an autoretarder (J.A. Woollam Co., Inc.). Measurements were performed with 0.05 eV steps in the 0.5-4.25 eV spectral range and for incidence angles between 65° and 85°.

The thickness of the film was modeled by fitting the data using a Cauchy layer on top of a native oxide coated Si surface in a non-absorbing region, typically at a photon energy > 1.1 eV. A point-by-point fit was then used for initial determination of the optical properties of the film. Once a good fit was obtained (low MSE value), the Cauchy model was then converted to a general oscillator (Genosc) model to ensure the correctness of the fit using physical oscillators

and to enforce the Kramers–Kronig relation, which connects the real and imaginary parts of the index of refraction. In the Genosc model, a series of the Lorentz and Drude oscillators is used to model the NiO_x layer. The Lorenz model incorporates interband absorptions with band tails, and the Drude model is especially useful in modeling the intraband absorption of the free carriers near the infrared region. The fitted refractive indices were physically Kramers-Kronig (K-K)-consistent (3).

Index grading, anisotropy, and thickness non-uniformity were added to the Genosc model. Grading in both the refractive index and extinction coefficient was implemented by modeling the layer assumed to have a grading consisting of multiple thin layers of the same material, each with optical properties that varied, to mimic grading due to the preparation method, where nucleation is typically involved. To improve the fitting accuracy, surface roughness was modeled by adding an effective medium approximation (EMA) layer of the material with 50% voids. The mean-squared error (MSE) between the model and the experimental data was low (< 6) for multiple samples with different thicknesses of NiO_x, and consideration of intermixing of SiO_x and NiO_x at the interfaces was therefore not required to obtain good fits to the data. Surface-adsorbed H_2O or OH groups as suggested by the Ni(III) peaks in the XPS spectra (Figure S2a) typically result in a lower refractive index of the existing surface layer than that of bulk NiO_x(4). This complicated thin surface layer was not needed explicitly in the modeling to obtain good fits to the data.

Total reflectance calculations:

The total reflectances of the semiconductor|NiO_x samples versus wavelength, with different NiO_x thickness varied from 0-300 nm with air or water as incident media and illuminated under various incidence angles, were calculated based on the propagation matrix of plane waves at dielectric interfaces. The Matlab function (*multidiel*) developed by Sophocles J.

Orfanidis from Rutgers University, was used to calculate the reflection responses of the isotropic non-lossy multilayer dielectric structures (5). Optical constants for water, crystalline Si, crystalline CdTe, and amorphous Si were adopted from previously reported values. The refractive indices for sputtered NiO_x were measured using spectroscopic ellipsometry described in the section above. The optical constant from the middle layer of the NiO_x was used for the calculation, averaging the graded index in the z-direction.

Surface recombination velocity:

Surface recombination velocity (*S*) measurements were made using a contactless microwave-conductivity apparatus that has been described previously (6, 7). A 20-ns pulsed-diode laser with a wavelength of 905 nm (OSRAM laser diode with an ETX-10A-93 driver) was used to generate electron-hole pairs in HTJ-Si. The lifetime of the photogenerated charge carriers was monitored using a PIN diode that detected the microwave radiation reflected from the sample. The HTJ-Si cell before and after NiO_x coating was measured. Samples were stored in N_2 glove box between measurements. Charge-carrier lifetimes and surface recombination velocities were calculated based on previous reports (6, 7).

Supporting figures:

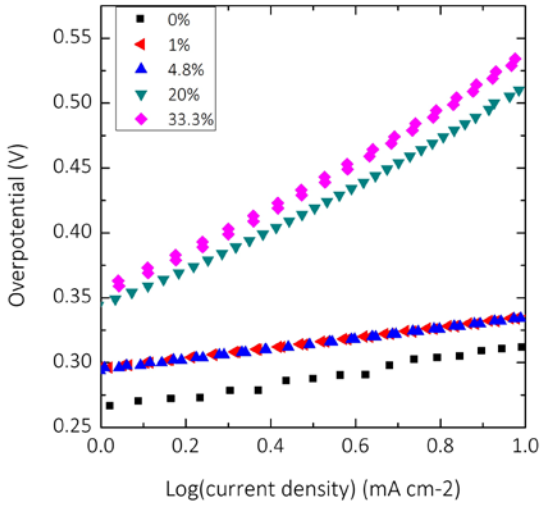

Figure S1. Tafel plot for samples prepared from different oxygen concentrations without substrate heating after resistance correction.

Figure S2c shows the crystallinity of the sputter-deposited film. When the oxygen concentration was 1%, the NiO_x film showed a comparable peak intensity in the (111), (200) and (220) directions, while films prepared with an oxygen concentration $\geqslant$4.8% showed a dominant peak in the (111) direction. Further increases in the temperature during sputter deposition did not change the preferred orientation, but produced a higher crystallinity in the resulting films. When the oxygen concentration was 1%, no metallic Ni peaks were observable at 2θ angles highlighted by the gray markers in Figure S2c, suggesting the formation of completely oxidized films under such conditions, consistent with the XPS observations (Figure S2a).

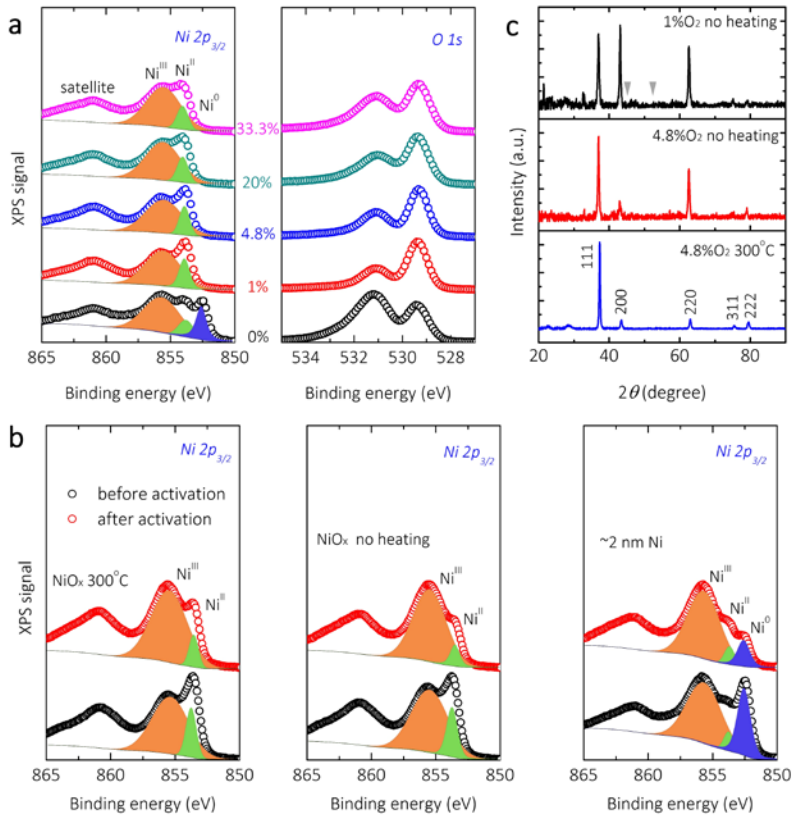

Figure S2. XPS data on p^+-Si|NiO_x samples prepared from different oxygen concentrations during sputter deposition (a), as well as on fresh and activated p^+-Si|NiO_x samples prepared with 4.8% O_2 concentration with and without substrate heating (b). For comparison, spectra are also displayed for 2 nm of sputtered Ni metal. Spectral regions containing the Ni $2p_{3/2}$ peaks (with Ni(II) at 853.86 eV (green area), Ni(III) at 855.69 eV (orange area), and metallic Ni at 852.55 eV (blue area)), and the O 1s peaks, are shown for NiO_x films deposited with oxygen concentrations that were varied between 0% (black curve) and 33.3% (magenta curve). (c) XRD data for NiO_x-coated p^+-Si (111) substrates prepared with different oxygen concentrations and substrate heating temperatures. The gray arrows indicate the diffraction-angle positions of crystalline Ni metal.

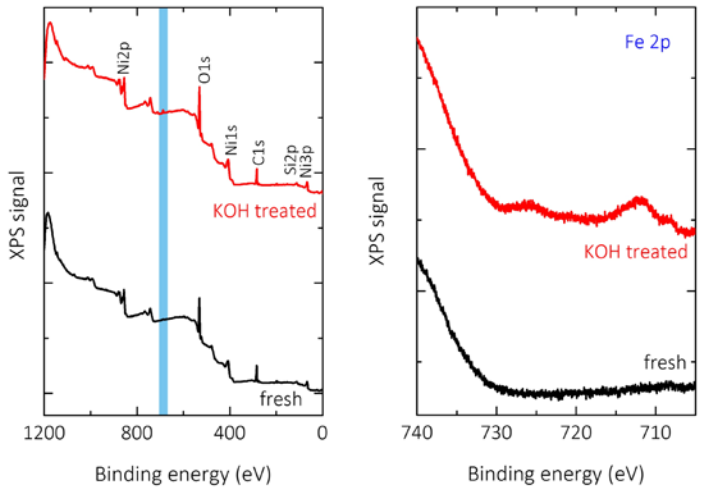

Figure S3. XPS survey scan and high resolution scan at Fe 2p region on Ni metal film coated non-photoactive p^+-Si before and after KOH treatment.

The refractive index in the region of 350–800 nm is 3.7–5.7 for Si, 4.1–5.2 for *a*-Si, and 3.0–3.4 for CdTe (Figure S4a). The minima of the total reflectance as well as the total reflection on these three substrates showed a trend of CdTe|NiO_x > c-Si|NiO_x > *a*-Si|NiO_x, consistent with the refractive index trend of CdTe < c-Si <*a*-Si for wavelengths > 400 nm. Tuning the physical thickness (*t*), and thus the optical thickness (*nt*), of the film affects the interference of light at different wavelengths (λ) and therefore affects the reflectance of the sample. Thin films (~ 3.5 nm) of NiO_x produced almost no change in the reflectance of polished crystalline Si (Figure S4d). However, increases up to 75 nm in the thickness of the NiO_x coating produced a pronounced reduction in the reflectance of the structure. Light interference became significant when the thickness of the NiO_x film was increased to 150 nm, with the reflection minima shifted to longer wavelengths.

The reflectance of the aforementioned bare and NiO_x-coated semiconductors should be reduced in water compared to air, because the optimum n_l needed for minimization of reflection

at a wavelength corresponding to its optical thickness ($4nt$) increases from 2 to 2.28 when the medium is switched from air (n=1) to water (n=1.3) ($n_l = \sqrt{n_i \times n_s}$,where n_l, n_i and n_s are refractive indices of the antireflection layer, the incident media, and the substrate, respectively). This increases the optimum n_l and gives better index matching in water (Figure S4e shows reflectance in air and water using Si as an example). The dependence of the reflectance at the air/semiconductor interface on the angle of incidence of the illumination was also broadly suppressed by 75-nm thick NiO_x coatings (Figure S4f), especially in the "reflectionless" region (~600 nm).

In the present study changes in the refractive index and extinction coefficient were not monitored in situ under operating conditions (8). However, based on the complex refractive indices reported for $Ni(OH)_2$ (1.38-0.06i) and NiOOH (1.41-0.07i) (4), and assuming that Ni atoms only within the top 10 nm of NiO_x were converted to catalytically active sites with a 50% volume expansion (9), the reflectance in the shorter-wavelength (< 600 nm) region will be suppressed (Figure S4g).

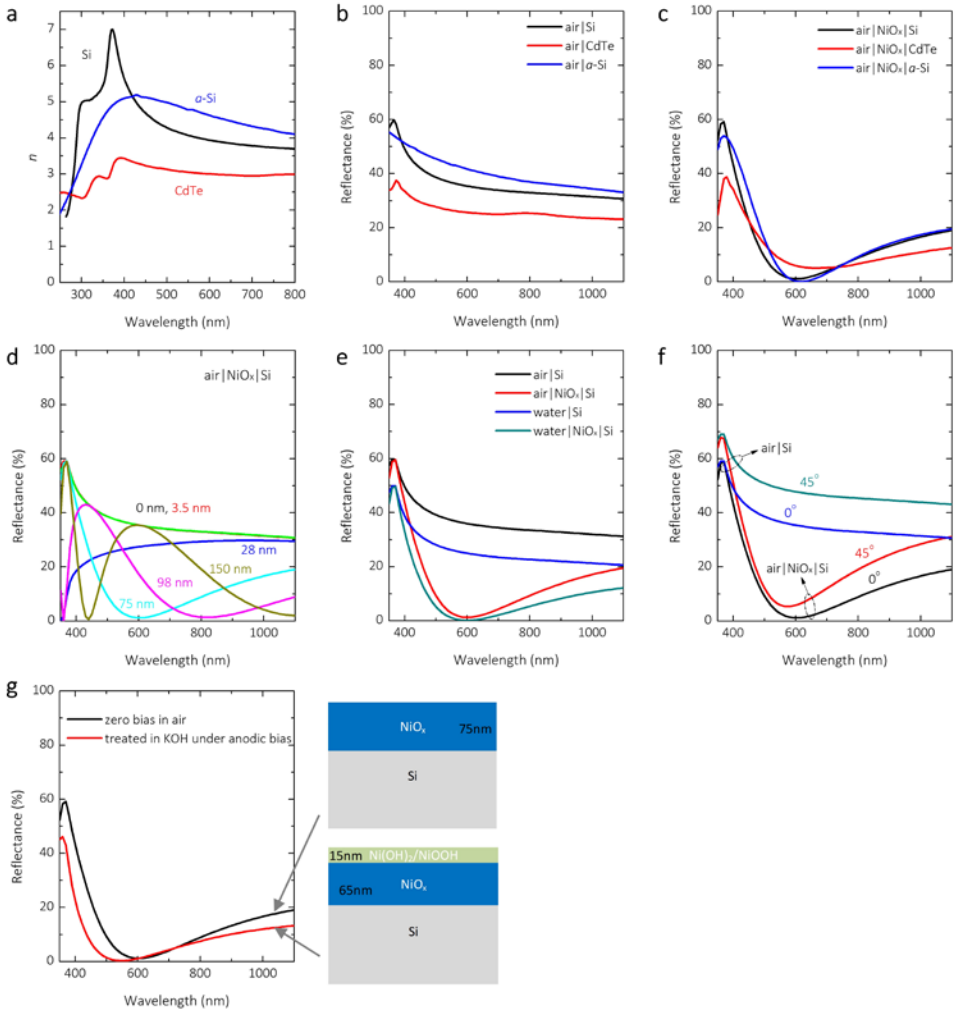

Figure S4. Calculated total reflectance on semiconductors with and without NiO_x films in different incident media. (a) Refractive indices of semiconductors including crystalline Si (black), crystalline CdTe (red), and *a*-Si (blue). (b) Reflectance from air|semiconductor interfaces based on the refractive index data of (a). (c) Reflectance from air|NiO_x|semiconductor interfaces. (d) Reflectance from air|NiO_x|Si interfaces with varied thickness of NiO_x. (e) Reflectance showing the effect of the incident media (water versus air) from media|NiO_x|Si and media|Si interfaces. (f) Reflectance showing the incident-angle effect at air|Si and air|NiO_x|Si interfaces. (g) Reflectance data showing the effect of a layer of $Ni(OH)_2$/NiOOH electrochemically converted from NiO_x.

The reflectance in panels b-e, g were obtained at normal incidence. The thicknesses of NiO_x layer in panels c, and e-g were 75 nm.

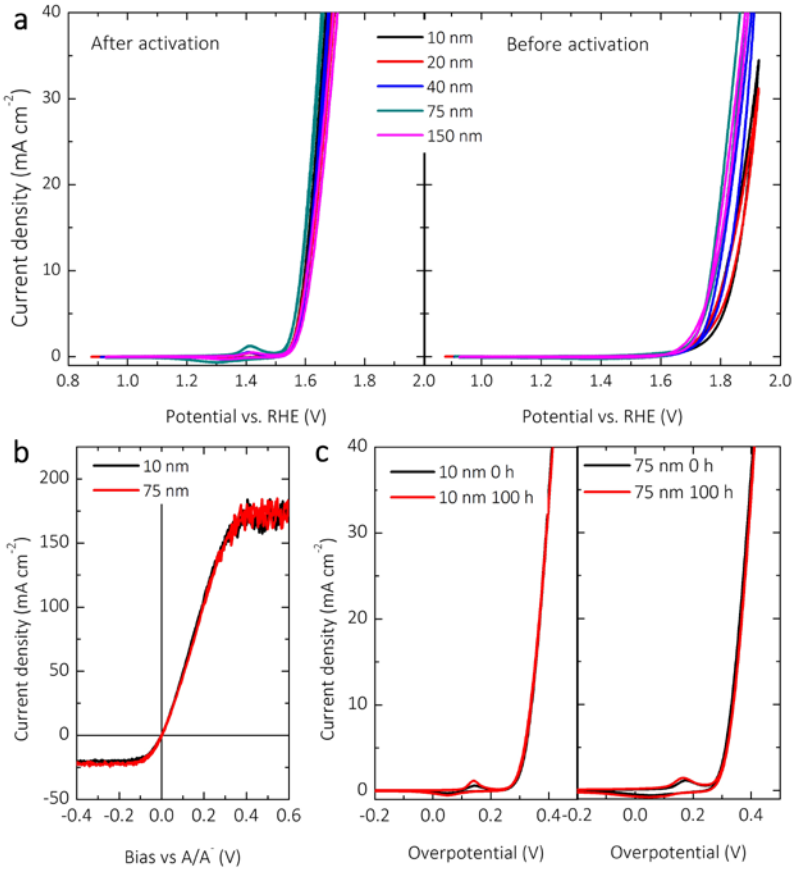

Figure S5. (a) *J-E* data for electrocatalytic water oxidation in 1.0 M KOH(aq), and (b) *J-E* data in 0.35 M $Fe(CN)_6^{3-}$/0.050 M $Fe(CN)_6^{4-}$ redox couple in 1.0 M KCl(aq), as a function of the thickness (10-150 nm) of the NiO_x film on p^+-Si substrates. (c) *J-E* data of the electrocatalytic activity of the NiO_x films in 1.0 M KOH(aq), before and after running at a constant current density of 30 mA cm^{-2} for 100 h, for films with thicknesses of 10 nm and 75 nm.

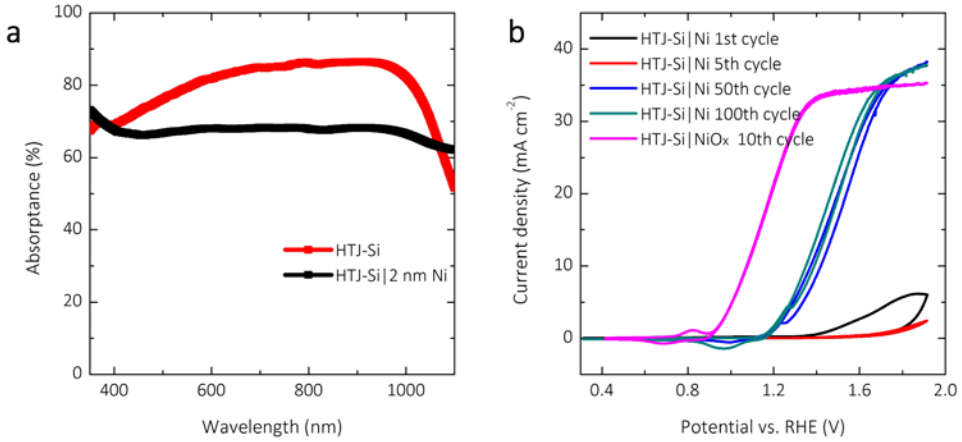

Figure S6. (a) Absorptance and (b) *J-E* behavior of a Ni metal coated HTJ-Si photoelectrode.

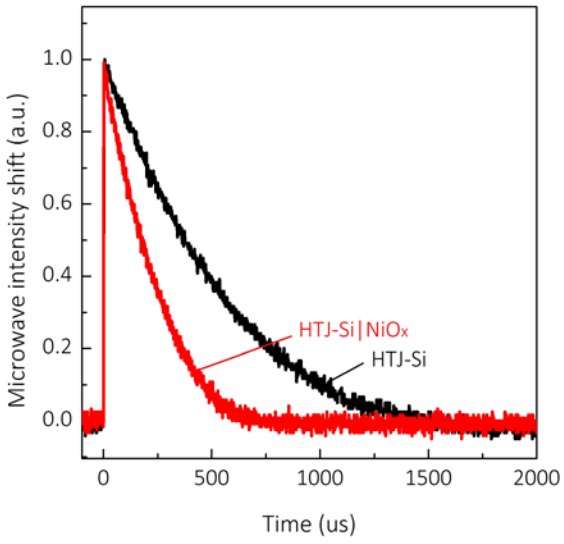

Figure S7. Representative time-resolved microwave conductivity (TRMC) decay signals for bare HTJ-Si and NiO_x coated HTJ-Si substrates.

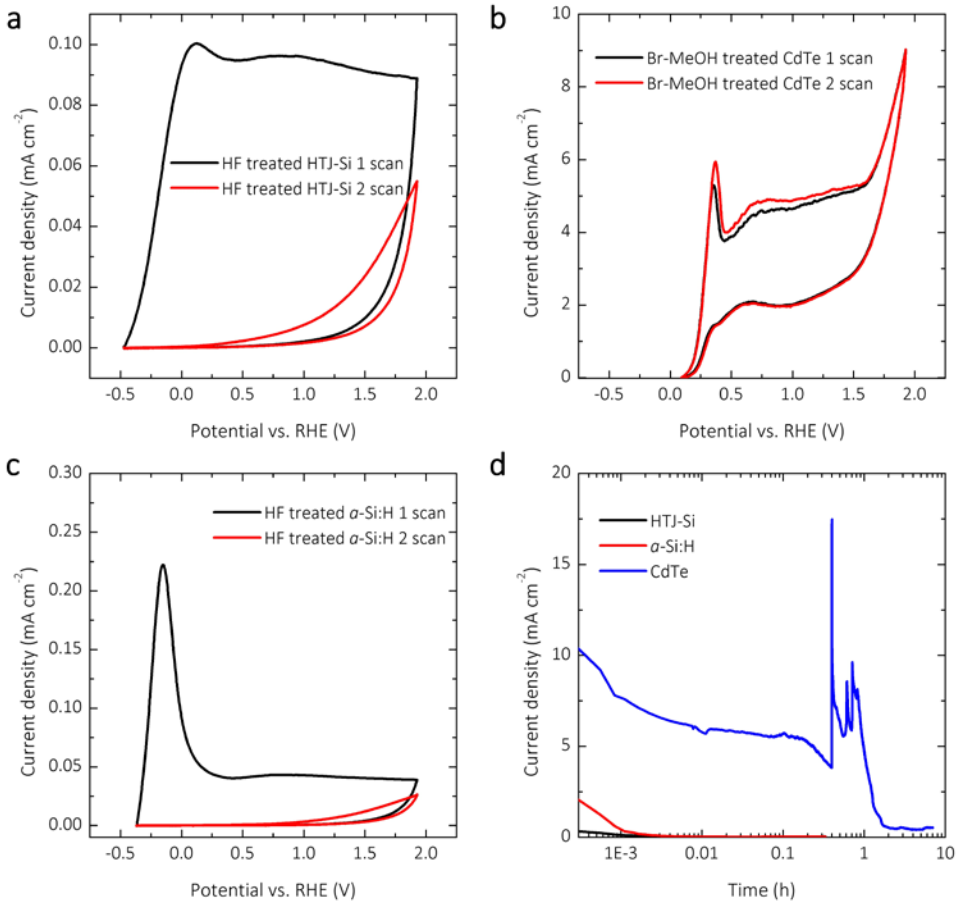

Figure S8. *J-E* data for HTJ-Si (a), CdTe (b) and *a*-Si:H (c) photoelectrodes without a NiO_x coating. (d) Chronoamperometry at 1.73 V vs. RHE of HTJ-Si, CdTe and *a*-Si:H photoelectrodes without a NiO_x coating. All of the measurements were performed in 1.0 M KOH(aq) under 100 mW cm^{-2} of simulated solar illumination.

Co-Pi (phosphate-containing CoO_x) has been used as a heterogeneous OER catalyst on various semiconductors (10-16). On FTO|Co-Pi (60 mC cm^{-2}) electrodes in 0.1 M K-Pi(aq), an overpotential of ~465 mV was observed at a current density of 1 mA cm^{-2} for the OER in the dark, consistent with the reported values (17). In alkaline media, the Co-Pi converted to the more active, but porous, known CoO_x OER electrocatalyst (Figure S9f). Consistently, the overpotential

at 1 mA cm^{-2} and 10 mA cm^{-2} decreased from 465 and 835 mV to 330 and 420 mV, respectively, when the 0.1 M phosphate buffered electrolyte, K-Pi(aq), was replaced by 1.0 M KOH(aq) (Figure S9a). In both electrolytes the observed overpotentials at 10 mA cm^{-2} were larger than the ~330 mV value reported herein for the NiO_x films in 1.0 M KOH(aq). At either pH, increases in the loading of the Co-Pi to obtain higher catalytic activity and thus improved fill factors in integrated photoelectrode structures resulted in an increase in light attenuation (Figure S9c and d), a significant reduction in the photocurrent (15), as well as deleterious increases in the resistivity (transport), and electrochromic coloration of the catalyst film. Moreover, Co-Pi coatings cannot be directly incorporated onto Si surfaces due to severe oxidation of the Si at the Co-Pi/Si interface as a result of the anodic catalyst-deposition process (16).

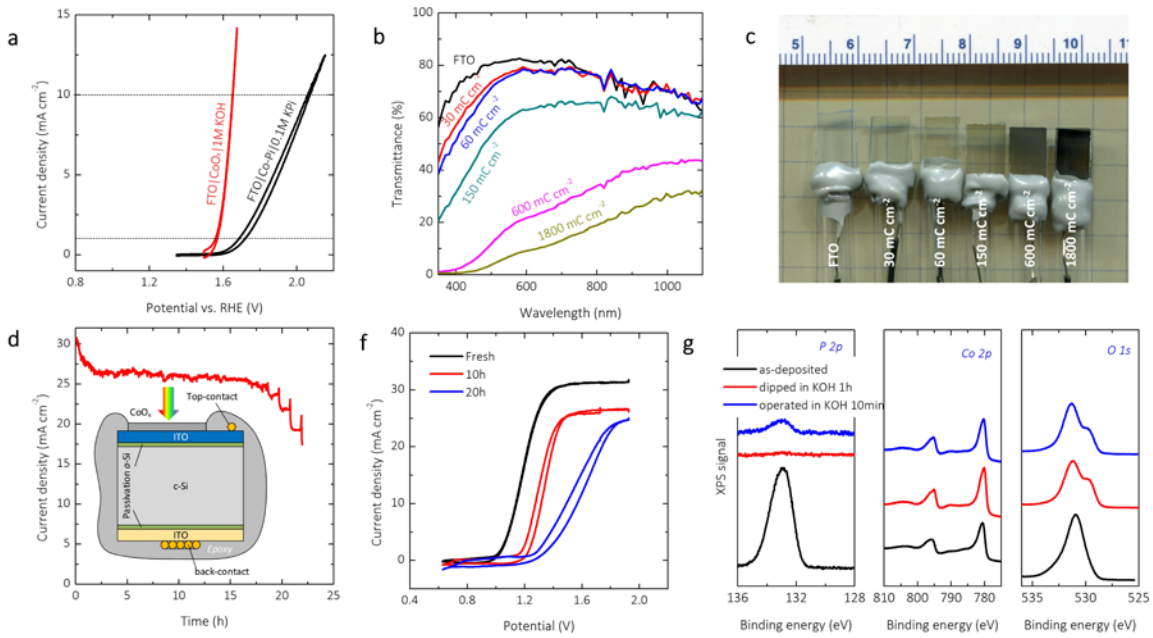

Figure S9. (a) *J-E* behavior of FTO|Co-Pi in 0.1 M K-Pi(aq) and FTO|CoO_x in 1 M KOH(aq) at a scan rate of 10 mV s^{-1}. The Co-Pi film was deposited by passing 60 mC cm^{-2} of charge. (b) Optical transmittance spectra of FTO glasses coated with different Co-Pi loadings (30-1800 mC cm^{-2}). (c) Optical images of Co-Pi deposited on FTO substrates by passing different amount of charges. (d) The stability of a HTJ-Si|ITO|CoO_x (60 mC cm^{-2}) photoelectrode that showed the

minimum optical loss, measured by contact through the back in the presence of 1-Sun of front-side illumination in 1.0 M KOH(aq). (e) *J-E* behavior showing the continual loss of photovoltage and a decrease of photocurrent for operation of a HTJ-Si|ITO|CoO_x (60 mC cm^{-2}) photoanode under these conditions. (f) XPS data on an as-deposited Co-Pi (black curves), on a Co-Pi film immersed in 1.0 M KOH (aq) for 1 h (red curves), and on a Co-Pi film operated at an anodic current density of 5 mA cm^{-2} for 10 min in 1.0 M KOH(aq) (blue curves). All three Co-Pi films were deposited on FTO glass by passing 60 mC cm^{-2} of charge, and were then independently processed and investigated spectroscopically. Spectral regions containing the P 2p peaks, Co 2p peaks and O 1s peaks are shown.

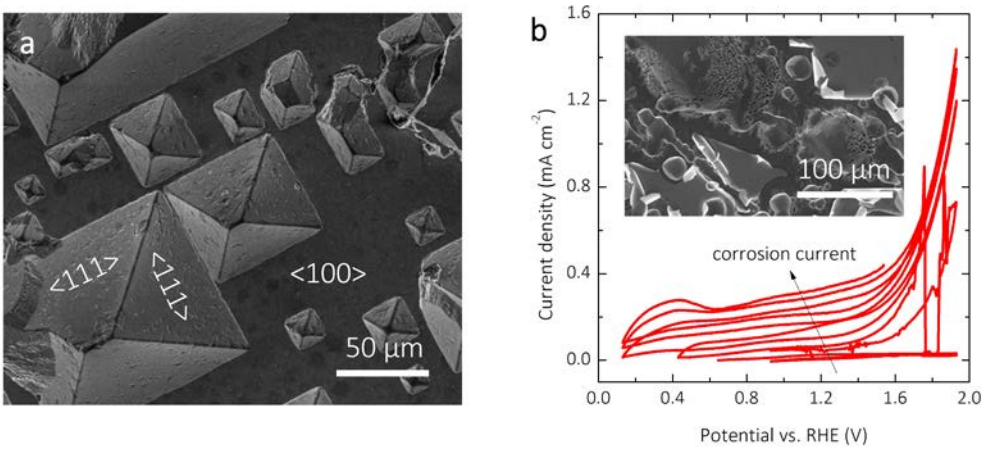

Figure S10. SEM images of (a) Si(100)|NiO_x immersed in 10.0 M KOH(aq) for 240 h at open circuit. (b) *J-E* data for an n^+-GaAs|NiO_x electrode showing an increasing current due to corrosion vs time. The inset depicts an SEM image obtained after anodic operation in 1.0 M KOH(aq) for 5 h, showing surface damage from the corrosion/dissolution of GaAs and peeling of the NiO_x layer. The thicknesses of the NiO_x layer in both cases were 75 nm.

Table S1. Analysis of the catalytic activity of NiO_x films prepared from different oxygen concentrations without substrate heating during sputtering. The data were corrected for solution resistance.

Oxygen concentration	**Tafel slope (1-10 mA cm^{-2})**	**Overpotential (mV) at 10 mA cm^{-2}**
0%	50	315
1%	40	335
4.8%	41	335
20%	171	517
33%	192	563

References:

1. Kumar A & Lewis NS (1990) Short-wavelength spectral response properties of semiconductor/liquid junctions. *J. Phys. Chem.* 94(15):6002-6009.
2. Gronet CM, *et al.* (1984) Correlation of the Photoelectrochemistry of the Amorphous Hydrogenated Silicon/Methanol Interface with Bulk Semiconductor Properties. *J. Electrochem. Soc.* 131(12):2873-2880.
3. Tompkins HG & McGahan WA (1999) *Spectroscopic Ellipsometry and Reflectometry: A User's Guide* (Wiley).
4. Wronkowska AA (1989) An ellipsometric investigation of nickel oxide films in alkaline solution: The multilayer film approach. *Surf. Sci.* 214(3):507-522.
5. Orfanidis SJ (2014) *Electromagnetic waves and antennas*.

6. Plass KE, Liu X, Brunschwig BS, & Lewis NS (2008) Passivation and Secondary Functionalization of Allyl-Terminated Si(111) Surfaces. *Chemistry of Materials* 20(6):2228-2233.

7. O'Leary LE, *et al.* (2013) Heck Coupling of Olefins to Mixed Methyl/Thienyl Monolayers on Si(111) Surfaces. *J. Am. Chem. Soc.* 135(27):10081-10090.

8. Gottesfeld S & Srinivasan S (1978) Electrochemical and optical studies of thick oxide layers on iridium and their electrocatalytic activities for the oxygen evolution reaction. *J. Electroanal. Chem. Interfacial Electrochem.* 86(1):89-104.

9. Sun K, *et al.* (2015) Stable Solar-Driven Water Oxidation to O_2(g) by Ni-oxide Coated Silicon Photoanodes *J. Phys. Chem. Lett.* 6:592-598.

10. Cong Y, *et al.* (2012) Synthesis of Ta_3N_5 Nanotube Arrays Modified with Electrocatalysts for Photoelectrochemical Water Oxidation. *J. Phys. Chem. C* 116(27):14541-14550.

11. Jeon TH, Choi W, & Park H (2011) Cobalt-phosphate complexes catalyze the photoelectrochemical water oxidation of $BiVO_4$ electrodes. *PCCP* 13(48):21392-21401.

12. Barroso M, *et al.* (2011) The Role of Cobalt Phosphate in Enhancing the Photocatalytic Activity of α-Fe_2O_3 toward Water Oxidation. *J. Am. Chem. Soc.* 133(38):14868-14871.

13. Steinmiller EMP & Choi K-S (2009) Photochemical deposition of cobalt-based oxygen evolving catalyst on a semiconductor photoanode for solar oxygen production. *Proc. Natl. Acad. Sci. USA* 106(49):20633-20636.

14. Pijpers JJH, Winkler MT, Surendranath Y, Buonassisi T, & Nocera DG (2011) Light-induced water oxidation at silicon electrodes functionalized with a cobalt oxygen-evolving catalyst. *Proc. Natl. Acad. Sci. USA* 108(25):10056-10061.

15. Reece SY, *et al.* (2011) Wireless Solar Water Splitting Using Silicon-Based Semiconductors and Earth-Abundant Catalysts. *Science* 334(6056):645-648.

16. Young ER, Costi R, Paydavosi S, Nocera DG, & Bulovic V (2011) Photo-assisted water oxidation with cobalt-based catalyst formed from thin-film cobalt metal on silicon photoanodes. *Energy Environ. Sci.* 4(6):2058-2061.

17. Surendranath Y, Kanan MW, & Nocera DG (2010) Mechanistic Studies of the Oxygen Evolution Reaction by a Cobalt-Phosphate Catalyst at Neutral pH. *J. Am. Chem. Soc.* 132(46):16501-16509.